Journal of Solid State Chemistry **165,** 381–392 (2002)
doi:10.1006/jssc.2002.9561, available online at http://www.idealibrary.com on IDEAL®

Structure and Conductivity of Perovskites $Sr_{1-x}La_xTi_{1-x}Cr_xO_3$

Guobao Li,*,[1] Xiaojun Kuang,* Shujian Tian,* Fuhui Liao,* Xiping Jing,*
Yoshiaki Uesu,† and Kay Kohn†

*College of Chemistry and Molecular Engineering, Peking University, Beijing 100871, China; and †Department of Physics, Waseda University, 3-4-1 Okubo, Shinjuku-ku, Tokyo 169-8555, Japan

Received November 8, 2001; in revised form February 11, 2002; accepted February 22, 2002

The $Sr_{1-x}La_xTi_{1-x}Cr_xO_3$ ($0 \le x \le 1$) system was synthesized at 1500°C for about 60 h. Their structures were analyzed by the use of powder X-ray diffraction data and Rietveld analysis software GSAS (General Structure Analysis System). Three solid solutions are found: cubic solid solution $Sr_{1-x}La_xTi_{1-x}Cr_xO_3$ ($0 \le x \le 0.168$, space group $Pm\bar{3}m$), rhombohedral solid solution $Sr_{1-x}La_xTi_{1-x}Cr_xO_3$ ($0.23 \le x \le 0.67$, space group $R\bar{3}c$) and orthorhombic solid solution $Sr_{1-x}La_xTi_{1-x}Cr_xO_3$ ($0.92 \le x \le 1$, space group *Pnma*). The conductivities of this series were measured mainly from 25 to 450°C. It was found that this series changed from dielectric material $SrTiO_3$ to semiconductor $LaCrO_3$ continuously. The highest conductive sample was found to be $Sr_{1-x}La_xTi_{1-x}Cr_xO_3$ with $x = 0.92$, whose conductivity at room temperature was about $5 \times 10^{-3}\ \Omega^{-1}\ cm^{-1}$.

1. INTRODUCTION

Various studies have been made on $SrTiO_3$ and doped $SrTiO_3$ in order to clarify their structural and physical properties, as they are fundamentally important oxides in solid-state physics. Pure $SrTiO_3$ belongs to cubic perovskite at room temperature and exhibits a structural phase transition to tetragonal phase at 105 K accompanied by rotations of oxygen octahedra. Although it remains paraelectric down to an extremely low temperature, several papers have shown that $SrTiO_3$ or doped $SrTiO_3$ could be a ferroelectric relaxor under certain conditions (1–9). In particular, relaxation behaviors were reported in the $Sr_{1-x}La_xTi_{1-x}Co_xO$ and $Sr_{1-x}La_xTi_{1-x}Ni_xO$ systems (10, 11). The motivation of the present series of study is to check whether these relaxation behaviors are also observed in the $Sr_{1-x}La_xTi_{1-x}Cr_xO_3$ system, compounds substituting both La and Cr into $SrTiO_3$.

[1] To whom correspondence should be addressed. E-mail: gblicn@263.net.

2. EXPERIMENTAL

The series $Sr_{1-x}La_xTi_{1-x}Cr_xO_3$ ($x = 0$, 0.05, 0.1, 0.2, 0.3, 0.4, 0.5, 0.6, 0.8, 0.86, 0.90, 0.92, 0.94, 0.96, 0.98, 1, named as SLTC01, SLTC02, …, SLTC16) has been synthesized from stoichiometric amounts of La_2O_3, $SrCO_3$, Cr_2O_3, and TiO_2 (high-purity grade). The oven-dried reagents were mixed and homogenized by grinding during about 30 min for total 6 g of mixtures with an agate mortar and a pestle. The mixtures were given three 6-h calcinations at 1400°C with intermediate grindings. They were then pressed into pellets to undertake six 10-h heat treatments at 1500°C followed by a furnace cooling each time with intermediate grinding and then were pressed again into pellets. All the treatments were carried out in air. The weights of the samples were monitored before and after heat treatments. The maximum difference was about 4 mg for the 6 g samples. Therefore, the compositions of the samples were considered to be the same as the initial ones.

X-ray diffraction data of the samples were obtained by using RAD-IC diffractometer employing Cu$K\alpha$ radiation ($\lambda_{CuK\alpha1} = 1.54056$ Å, $\lambda_{CuK\alpha2} = 1.54440$ Å) with an Ni filter, operated with 40 kV, 20 mA, and a continuous scanning method with 0.2°/min, and RINT diffractometer employing Fe$K\alpha$ radiation ($\lambda_{FeK\alpha1} = 1.93604$ Å, $\lambda_{FeK\alpha2} = 1.93998$ Å) with an Mn filter operated with 40 kV, 20 mA, and a step scanning method with $\Delta 2\theta = 0.026°$, $\Delta t = 5$ s. The scanning 2θ range was 20–140° for Cu$K\alpha$ radiation, or 24–150° for Fe$K\alpha$ radiation.

The X-ray diffraction data were analyzed by using GSAS software to obtain the lattice parameters. Acceptable fittings between the experimental data and the proposed models were obtained with $R_p < 4.0\%$, $R_{wp} < 5.0\%$ for all the data.

AC impedance data were obtained from HP4192A impedance analyzer. The two faces of the pressed sample were pasted with Pt paster. The frequency range is 5 Hz–12 MHz. The temperature range is 25–450°C.

0022-4596/02 $35.00

TABLE 1
The Comparison of the Structural Information of the $Sr_{1-x}La_xTi_{1-x}Cr_xO_3$ ($0 \le x \le 1$) System Reported

	The presenting phases		
x	Mitchell and Chakhmouradian (12)[a]	Kennedy *et al.* (13)[b]	This work[c]
0	$Pm\bar{3}m$	$Pm\bar{3}m$	$Pm\bar{3}m$
0.1	$I4/mcm$	$Pm\bar{3}m$	$Pm\bar{3}m$
0.2	$I4/mcm$	$Pm\bar{3}m$	$Pm\bar{3}m + R\bar{3}c$
0.3	$Pnma$	$R\bar{3}c$	$R\bar{3}c$
0.4	$Pnma$	$R\bar{3}c$	$R\bar{3}c$
0.5	$Pnma$	$R\bar{3}c$	$R\bar{3}c$
0.6	$Pnma$	$R\bar{3}c$	$R\bar{3}c$
0.8	$Pnma$	$R\bar{3}c$	$R\bar{3}c + Pnma$
0.9	$Pnma$	$Pnma$	$R\bar{3}c + Pnma$
1.0	$Pnma$	$Pnma$	$Pnma$

[a] Synthesized at 1350°C for 24 h.
[b] Synthesized at 1500°C for 48 h.
[c] Synthesized at 1500°C for 60 h.

3. STRUCTURE ANALYSIS

Some differences were reported for the structural information of the $Sr_{1-x}La_xTi_{1-x}Cr_xO_3$ ($0 \le x \le 1$) system (12, 13) as shown in Table 1. Our work confirmed that at room temperature the series $Sr_{1-x}La_xTi_{1-x}Cr_xO_3$ ($0 \le x \le 1$) was composed of three solid solutions and two two-phases areas. The solid solutions were cubic $Sr_{1-x}La_xTi_{1-x}Cr_xO_3$ ($0 \le x \le 0.168$), rhombohedral $Sr_{1-x}La_xTi_{1-x}Cr_xO_3$ ($0.23 \le x \le 0.67$) and orthorhombic $Sr_{1-x}La_xTi_{1-x}Cr_xO_3$ ($0.92 \le x \le 1$). Between them there are the corresponding two-phase regions. These results agree well with that of Kennedy *et al.* (13) except for some details.

3.1. Cubic Solid Solution $Sr_{1-x}La_xTi_{1-x}Cr_xO_3$

It is well known that at room temperature $SrTiO_3$ has a cubic perovskite structure (space group $Pm\bar{3}m$) (14). The diffraction pattern of $SrTiO_3$ synthesized in the present work can be well refined by the $Pm\bar{3}m$ structural model with Ti at (0.5, 0.5, 0.5), Sr at (0, 0, 0) and O at (0.5, 0.5, 0) sites with $R_p = 3.6\%$ and $R_{wp} = 4.4\%$. The refined lattice parameter [$a = 3.9051(1)$ Å] is closer to the previously obtained values (12, 15).

It was found that the diffraction patterns of SLTC02 and SLTC03 ($Sr_{1-x}La_xTi_{1-x}Cr_xO_3$ with $x = 0.05$, 0.1) could also be refined well by the $Pm\bar{3}m$ structural model with Ti and Cr at (0.5, 0.5, 0.5), Sr and La at (0, 0, 0), and O at (0.5, 0.5, 0) sites. The corresponding lattice parameters are 3.9036(1) and 3.9020(1) Å, respectively.

As for the sample SLTC04 ($Sr_{1-x}La_xTi_{1-x}Cr_xO_3$ with $x = 0.2$), the X-ray diffraction data could be fitted well using

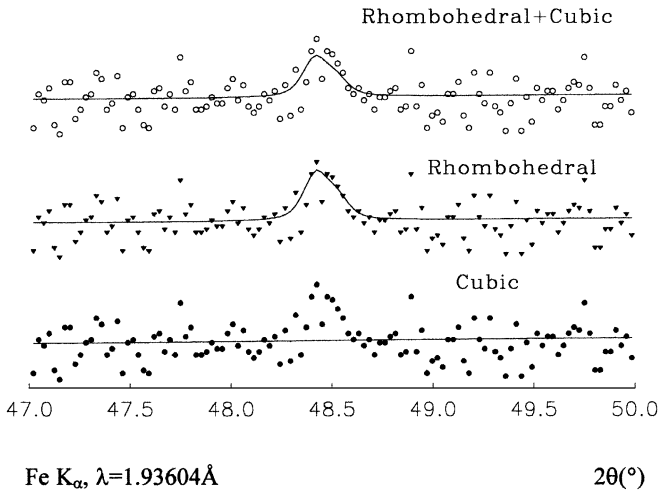

FIG. 1. The fitting results of the sample SLTC04 from different models.

three models: (1) cubic model with $a_c = 3.8992(1)$ Å, $R_{wp} = 4.48\%$ and $R_p = 3.47\%$; (2) cubic plus rhombohedral model with $a_c = 3.8999(1)$ Å, $a_h = 5.5156(1)$ Å, $c_h = 13.5014(1)$ Å, $R_{wp} = 4.47\%$ and $R_p = 3.46\%$; (3) rhombohedral model $a_h = 5.5135(1)$ Å, $c_h = 13.5118(1)$ Å, $R_{wp} = 4.49\%$ and $R_p = 3.48\%$. It was difficult to say which was better. However, the rhombohedral phase had a diffraction peak around 48.5° while using Fe$K\alpha$ radiation as shown in Fig. 1. A peak actually existed around 48.5° in the X-ray diffraction data of the sample SLTC04. Therefore, it was reasonable to say that there was a rhombohedral phase in the sample SLTC04. We preferred to think that there were two phases, cubic phase and rhombohedral phase, in this

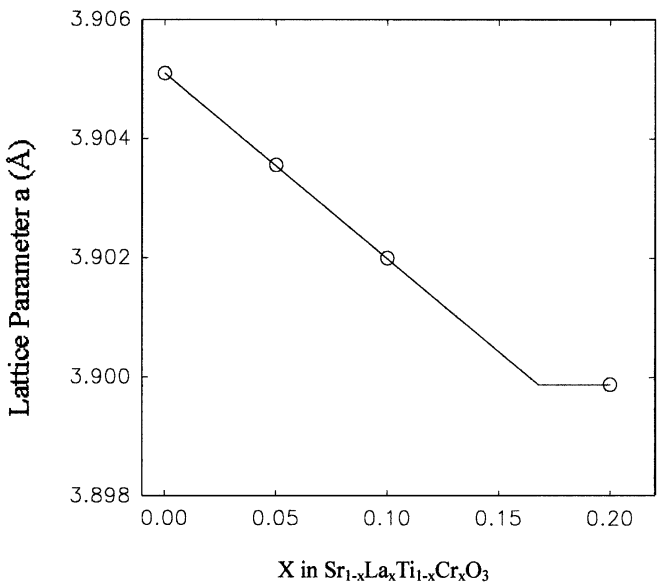

FIG. 2. Variation of the lattice parameter a of the cubic phase with the average composition ratio x. x is the ratio of La/(La + Sr) in the sample.

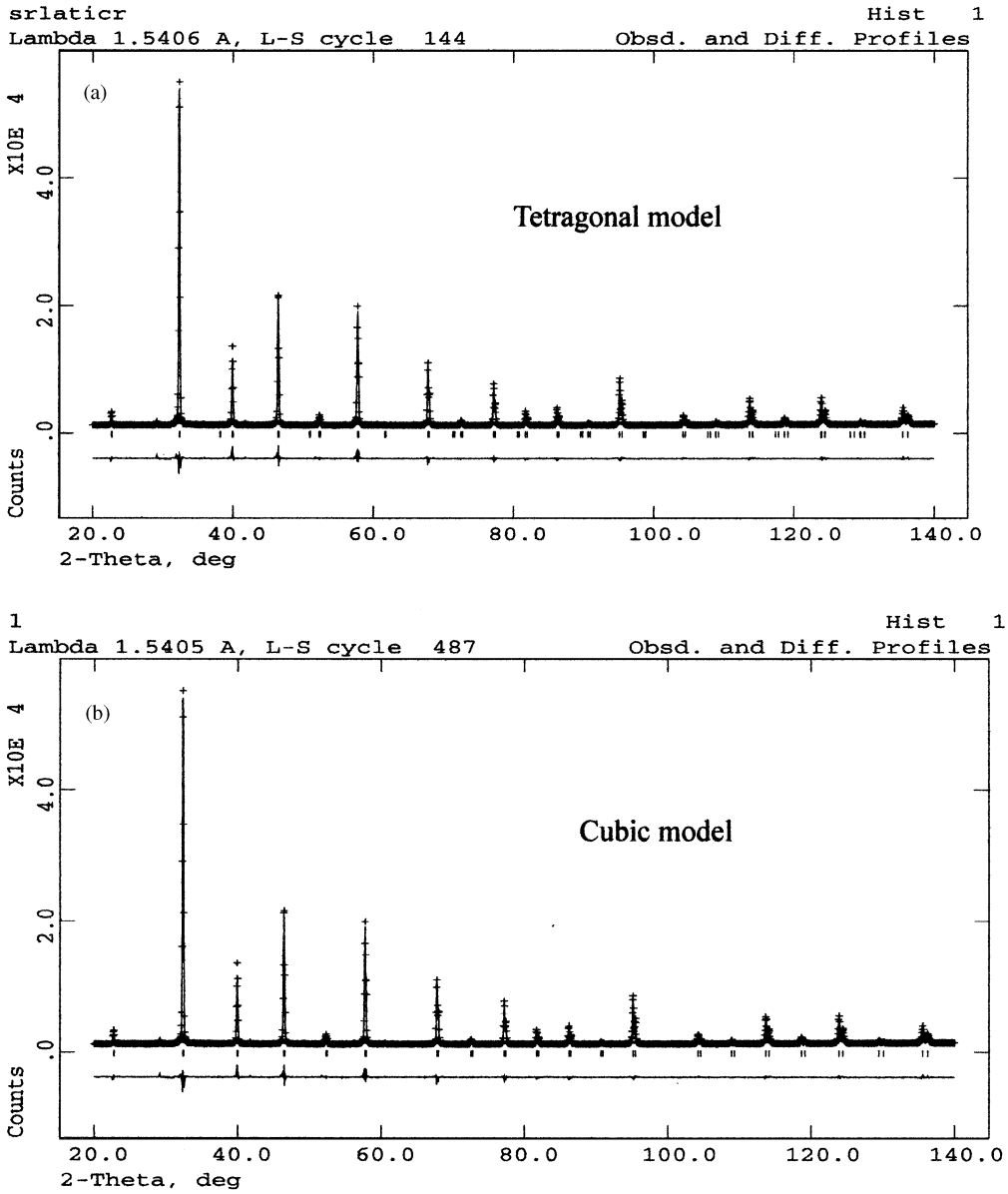

FIG. 3. The comparison of the fitting patterns of the sample SLTC03 in the range 20–140° with different models: (A) tetragonal model ($I4/mcm$, $a_t = 5.5180(1)$ Å, $c_t = 7.8063(1)$ Å, $R_{wp} = 3.96\%$, $R_p = 2.53\%$); and (B) cubic model ($Pm\bar{3}m$, $a_c = 3.9020(1)$ Å, $R_{wp} = 3.93\%$, $R_p = 2.54\%$).

sample. The more detailed reasons are shown in the next section.

Figure 2 shows the relationship of the lattice parameter a of the cubic solid solution $Sr_{1-x}La_xTi_{1-x}Cr_xO_3$ with composition parameter x of the samples. This relationship agreed well with Vegard's law (16, 17):

$$a_x^c = a_0^c(1 - x) + a_1^c x. \quad [1]$$

Here, a_x^c, a_0^c and a_1^c were the lattice parameters of the cubic $Sr_{1-x}La_xTi_{1-x}Cr_xO_3$, $SrTiO_3$ and the supposedly cubic $LaCrO_3$; $a_0^c = 3.9051$ Å and $a_1^c = 3.8740$ Å. Following this relationship, the maximum x for the cubic $Sr_{1-x}La_xTi_{1-x}Cr_xO_3$ was found to be 0.168 at room temperature.

However, Mitchell and Chakhmouradian (12) had shown that the solid solutions $Sr_{1-x}La_xTi_{1-x}Cr_xO_3$ with $0.1 \leq x \leq 0.2$ were of tetragonal structure. In fact, for example, the powder X-ray diffraction data of the sample SLTC03 (with $x = 0.1$) could be fitted well using the tetragonal model ($I4/mcm$, $a_t = 5.5180(1)$ Å, $c_t = 7.8063(1)$ Å, $R_{wp} = 3.96\%$, $R_p = 2.53\%$) and cubic model ($Pm\bar{3}m$, $a_c = 3.9020(1)$ Å, $R_{wp} = 3.93\%$, $R_p = 2.54\%$). Figures 3–5 show the differences of the fitted results between the tetragonal and cubic model. Obviously, the tetragonal model gave more expected

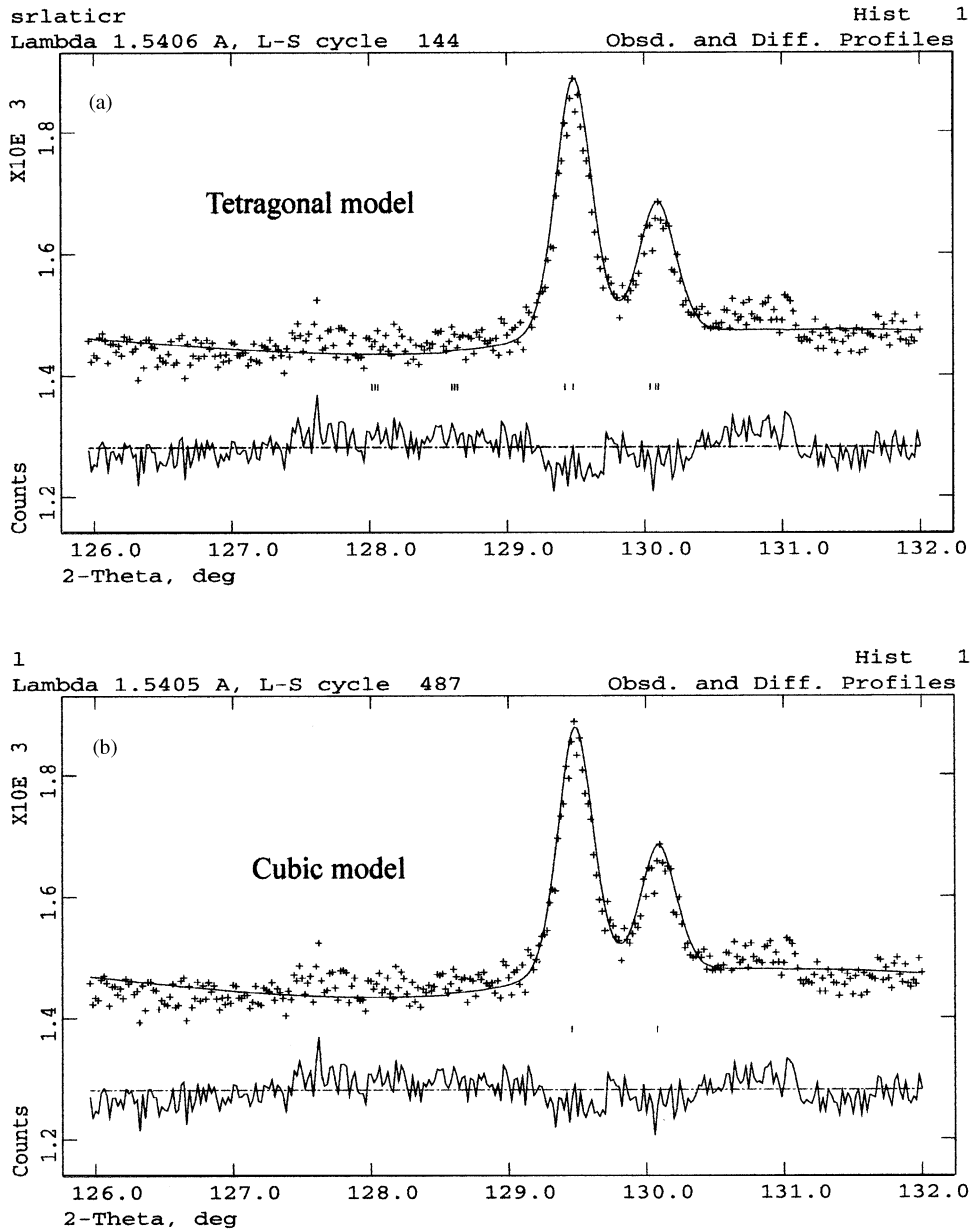

FIG. 4. The comparison of the fitting patterns of the sample SLTC03 in the range 126–132° with two models: (A) tetragonal model; and (B) cubic model. Some supperlattice peaks expected by the tetragonal model was not observed.

peaks than the cubic model, but these additional peaks were not found in the observed data. In addition, $c_t/a_c = 2.0006$, $a_t/a_c = 1.41415$, $\sqrt{2} = 1.41421$. This meant that it was better to choose the cubic model to describe the structure of the solid solution $Sr_{1-x}La_xTi_{1-x}Cr_xO_3$ around $x = 0.1$ at room temperature.

3.2. Rhombohedral Solid Solution $Sr_{1-x}La_xTi_{1-x}Cr_xO_3$

It was found that the diffraction patterns of SLTC05 and SLTC08 ($Sr_{1-x}La_xTi_{1-x}Cr_xO_3$ with $x = 0.30$, 0.40, 0.50, 0.60) could be refined well by the $R\bar{3}c$ structural model with Sr and La at 6*a* (0, 0, 0.25), Ti and Cr at 6*b* (0, 0, 0), and O at 18*e* ($x \approx 0.5285$, 0, 0.25) sites. The corresponding lattice parameters are listed in Table 2. This agreed with the results reported by Kennedy *et al.* (13).

Mitchell and Chakhmouradian (12) had suggested that the solid solutions $Sr_{1-x}La_xTi_{1-x}Cr_xO_3$ with $x = 0.30$, 0.40, 0.50, 0.60 were of orthorhombic structure with the space group *Pnma*. In order to check this possibility, the data were tried to fit with this model. The fitted results forced us to reject this model. For example, for the power

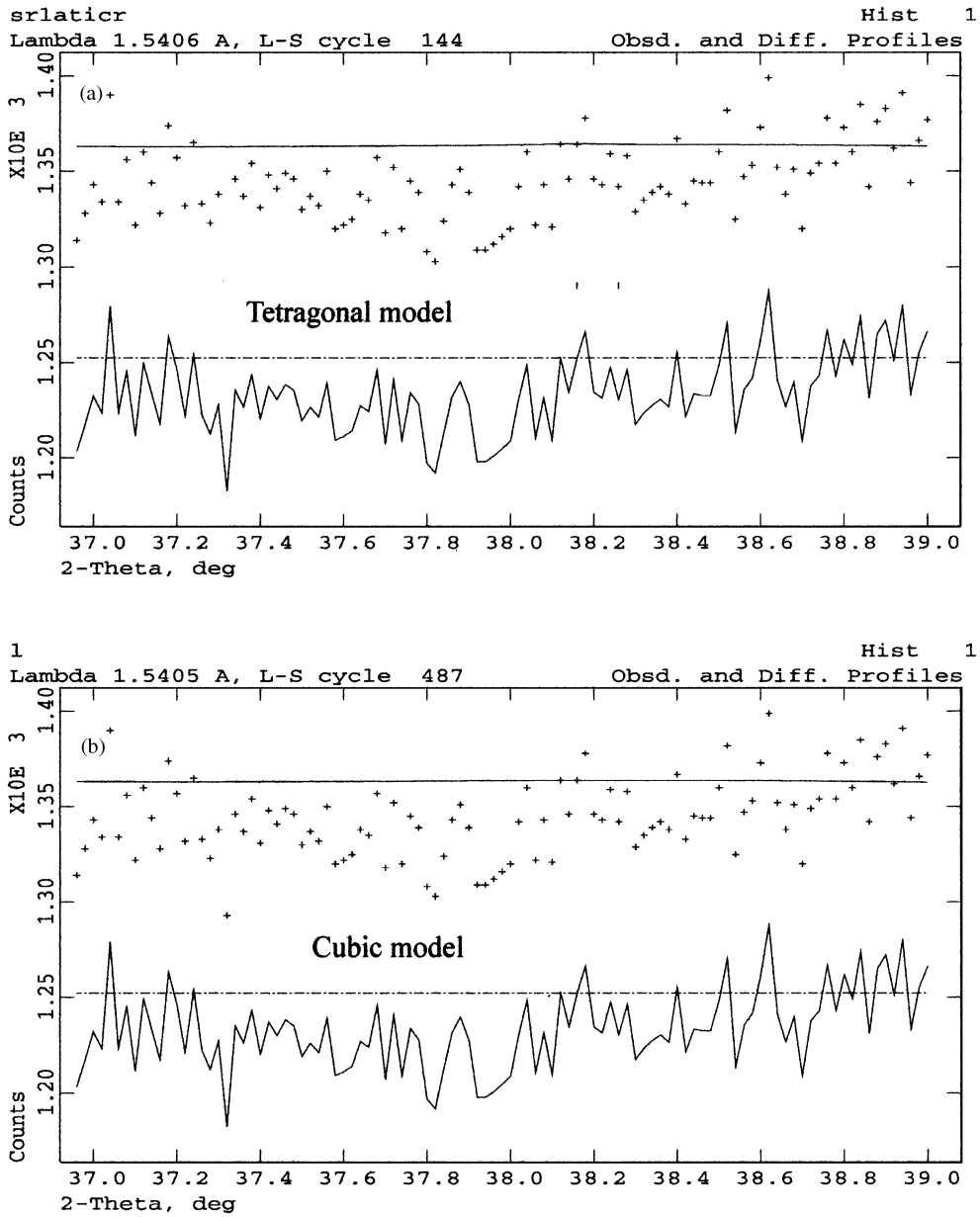

FIG. 5. The comparison of the fitting patterns of the sample SLTC03 in the range 37–39° with two models: (A) tetragonal model; and (B) cubic model. The supperlattice peaks expected by the tetragonal model was not observed.

X-ray diffraction data of the sample SLTC08 with $x = 0.60$, the orthorhombic model gave a fitting result of $a_o = 5.4810(2)$ Å, $b_o = 7.7781(4)$ Å, $c_o = 5.5169(2)$ Å, $R_{wp} = 9.61\%$ and $R_p = 6.21\%$. Usually, this was acceptable. However, the rhombohedral model gave a better result of $a_h = 5.5108(1)$ Å, $c_h = 13.4073(1)$ Å, $R_{wp} = 4.32\%$ and $R_p = 3.12\%$. In addition, the rhombohedral model could explain all the peaks observed as shown in Fig. 6. Therefore, the rhombohedral model was accepted.

TABLE 2
The Lattice Parameters *a* and *c* of the Rhombohedral Solid Solution $Sr_{1-x}La_xTi_{1-x}Cr_xO_3$

Name	SLTC05	SLTC06	SLTC07	SLTC08
X	0.30	0.40	0.50	0.60
A (Å)	5.5141(1)	5.5129(1)	5.5120(1)	5.5108(1)
C (Å)	13.4848(1)	13.4568(1)	13.4348(1)	13.4073(1)

Now let us discuss the question related to the sample SLTC04 ($x = 0.20$). As mentioned in the above section, it may be a single-phase sample of rhombohedral structure, or a two-phase sample composed of a cubic phase and a rhombohedral phase. After the data of this sample were plotted together with other data, it was easy to accept that this

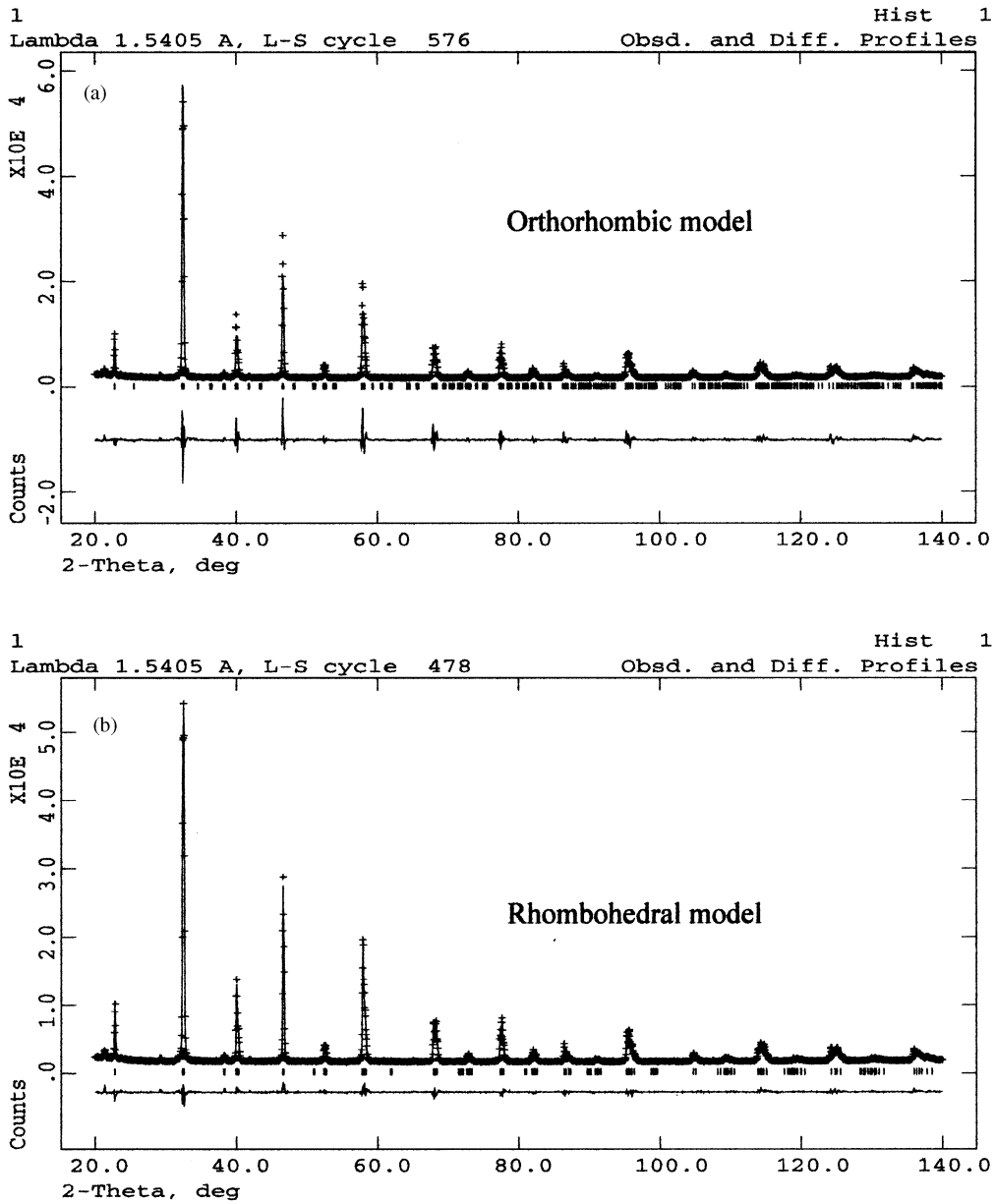

FIG. 6. The comparison of the fitting patterns of the sample SLTC08 in the range 20–140° with different models: (A) orthorhombic model ($a_o = 5.4810(2)$ Å, $b_o = 7.7781(4)$ Å, $c_o = 5.5169(2)$ Å, $R_{wp} = 9.61\%$, $R_p = 6.21\%$); and (B) rhombohedral model ($a_h = 5.5108(1)$ Å, $c_h = 13.4073(1)$ Å, $R_{wp} = 4.32\%$, $R_p = 3.12\%$).

sample was a two-phase sample as shown in Fig. 7. The main reason was the departure of the data of this sample from Eq. [2]. According to the same reason, samples SLTC09, SLTC10, and SLTC11 (corresponding to $Sr_{1-x}La_xTi_{1-x}Cr_xO_3$ with $x = 0.8$, 0.86, 0.90) were treated as two-phase samples.

The relationship of the lattice parameters of the rhombohedral solid solution $Sr_{1-x}La_xTi_{1-x}Cr_xO_3$ with composition parameter x of the samples, also agreed well with Vegard's law (16, 17):

$$a_x^r = a_0^r(1 - x) + a_1^r x. \quad [2]$$

Here a_x^r, a_0^r and a_1^r are the lattice parameters of the rhombohedral $Sr_{1-x}La_xTi_{1-x}Cr_xO_3$, the supposed rhombohedral $SrTiO_3$ and the supposed rhombohedral $LaCrO_3$; $a_0^r = 3.9057$ Å and $a_1^r = 3.8762$ Å. Following this relationship, the minimum x and the maximum x for the rhombohedral $Sr_{1-x}La_xTi_{1-x}Cr_xO_3$ was found to be 0.23(1) and 0.67(1) at room temperature.

Kennedy *et al.* (13) reported that the sample $Sr_{1-x}La_xTi_{1-x}Cr_xO_3$ with $x = 0.9$ should be orthorhombic at room temperature. A phase transition between orthorhombic and rhombohedral phase occurred around 150°C. In our analysis, we found that the diffraction peaks come

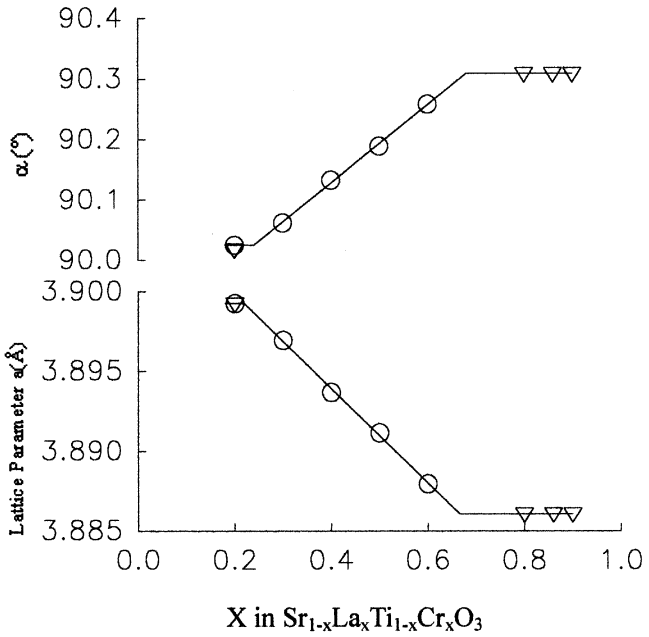

FIG. 7. Variation of the lattice parameters a and α of the rhombohedral phase with the average composition ratio x. x is the ratio of La/(La + Sr) in the sample. ∇, the lattice parameters a and α obtained under the two-phase model; ○, the lattice parameters a and α obtained under the one-phase model.

from orthorhombic and rhombohedral phase overlapped heavily as shown in Fig. 8. There were still some differences found in the two ranges of 2θ as shown in Fig. 9. The upper short line in Fig. 9 indicated the diffraction peaks expected in the orthorhombic model. The lower short line indicated the diffraction peaks expected by the rhombohedral model. By carefully comparing the observed peaks and the expected peaks using different models, it was easy to believe that the sample $Sr_{1-x}La_xTi_{1-x}Cr_xO_3$ with $x = 0.9$ had two phases.

3.3. Orthorhombic Solid Solution $Sr_{1-x}La_xTi_{1-x}Cr_xO_3$

The compound $LaCrO_3$ was orthorhombic (18–20) at room temperature. The powder X-ray diffraction data of $LaCrO_3$ synthesized in this work could be refined well by using *Pnma* with $R_p = 1.9\%$, $R_{wp} = 2.4\%$. The unit-cell parameters and the atomic coordinates obtained for $LaCrO_3$ in the present work were in a reasonable agreement with those reported in the previous studies (12, 20–22) (Table 3).

The samples SLTC13–STLC16 with a small amount of La and Cr to be substituted into Sr and Ti, respectively, were found to exhibit a single phase having the same orthorhombic structure as $LaCrO_3$ with $R_p \leq 1.9\%$, $R_{wp} \leq 2.4\%$ for all these samples. The corresponding lattice parameters are presented in Table 4. As shown in Fig. 10, the relationship between the lattice parameters and the composition x of the solid solution $Sr_{1-x}La_xTi_{1-x}Cr_xO_3$ agreed well with Vegard's law (16, 17). The minimum x was found to be 0.92(1).

4. CONDUCTIVITY

Usually, the impedance spectra of ceramics contained the information of the bulk, grain boundary and electrode (23). The contribution from the grain boundary and the electrode

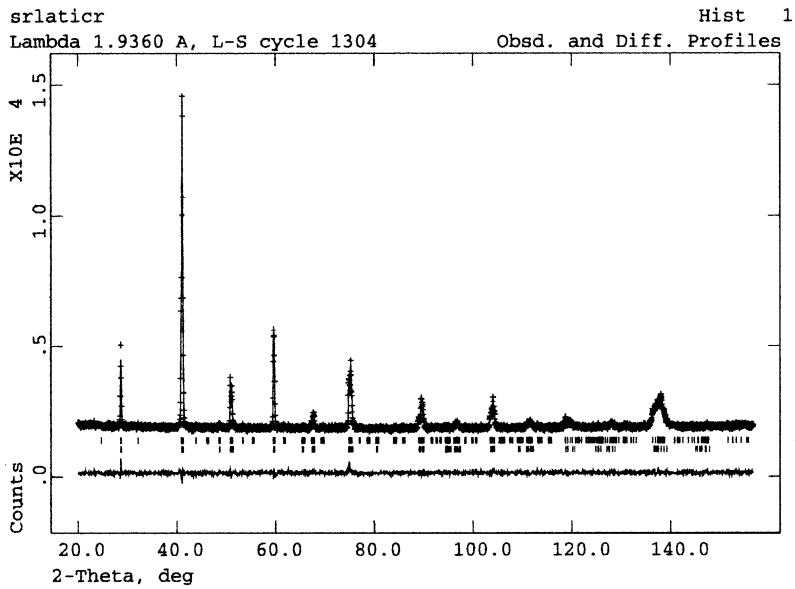

FIG. 8. The observed and fitting patterns of the sample SLTC11 in the range 24–156°. Two phases, the rhombohedral phase ($a_h = 5.5106(1)$ Å, $c_h = 13.3889(1)$ Å) and the orthorhombic phase ($a_o = 5.4792(1)$ Å, $b_o = 7.7567(2)$ Å, $c_o = 5.5185(1)$ Å) were used in the fitting. The lower short line indicated the peaks expected by the rhombohedral phase, the upper short line indicated the peaks expected by the orthorhombic phase.

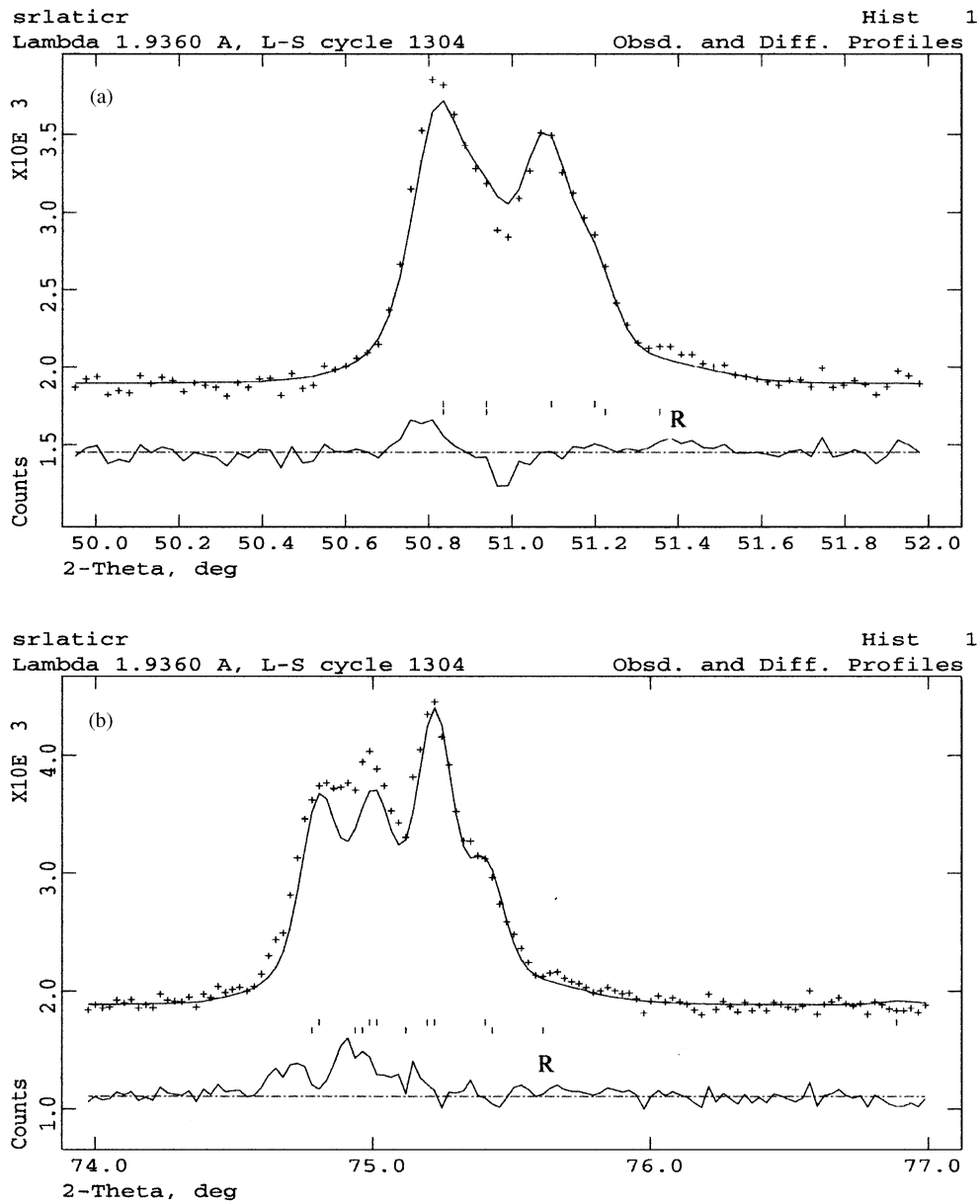

FIG. 9. The two enlarged parts of Fig. 8. (A) The range 50–52°; and (B) the range 74–77°. Some small peaks showed the existence of the rhombohedral phase as indicated by the symbol R.

were different with different treatments of the samples. In order to give a comparable result, only the bulk conductivity was discussed below. They were presented in several figures to show clearly the difference in different samples.

Figure 11 showed typical impedance spectra of the sample SLTC01 ($SrTiO_3$). According to the work of Abrantes *et al.* (23), using the software of EQUIVCRT (24), it was easy to obtain the bulk resistance of the sample. Figure 12 showed the bulk conductivity of samples SLTC01–SLTC04. They were of cubic structure at room temperature expect SLTC04. From these data, the activation energies were found to be 1.05, 0.29, 0.28 and 0.27 eV for SLTC01–SLTC04, respectively.

The bulk conductivity activation energy of $SrTiO_3$ prepared by us was almost the same as that reported by Abrantes *et al.* (25), whose result was 0.99 eV. After doping with $LaCrO_3$, the bulk conductivity of the sample increased considerably with the increase in the amount of the dopant in the sample, as shown in Fig. 12. The bulk conductivity activation energy changed to 0.28(1) eV.

TABLE 3
The Structure Information for $LaCrO_3$ (*Pnma*)

		Khattak and Cox (20)	Mitchell and Chakhmouradian (12)	Tesuka *et al.* (22)	This work
a (Å)		5.483	5.4797(1)	5.4813(1)	5.4803(1)
b (Å)		7.765	7.7588(2)	7.7611(1)	7.7599(1)
c (Å)		5.520	5.5163(1)	5.5181(1)	5.5168(1)
La	*X*	0.0196(4)	0.0191(2)	0.019(1)	0.0206(1)
	Y	0.2500	0.2500	0.2500	0.2500
	Z	− 0.0046(5)	− 0.0026(5)	0.006(1)	− 0.0064(1)
Cr	*X*	0.0000	0.0000	0.0000	0.0000
	Y	0.0000	0.0000	0.0000	0.0000
	Z	0.5000	0.5000	0.5000	0.5000
O1	*X*	0.4935(6)	0.496(2)	0.494(3)	0.5084(1)
	Y	0.2500	0.250	0.250	0.25000
	Z	0.0676(4)	0.059(3)	− 0.046(5)	0.0221(1)
O2	*X*	0.2265	0.233(3)	0.271(4)	0.2437(1)
	Y	0.5338	0.537(2)	0.031(2)	0.5065(1)
	Z	0.2265(3)	0.228(3)	− 0.281(3)	0.2434(1)

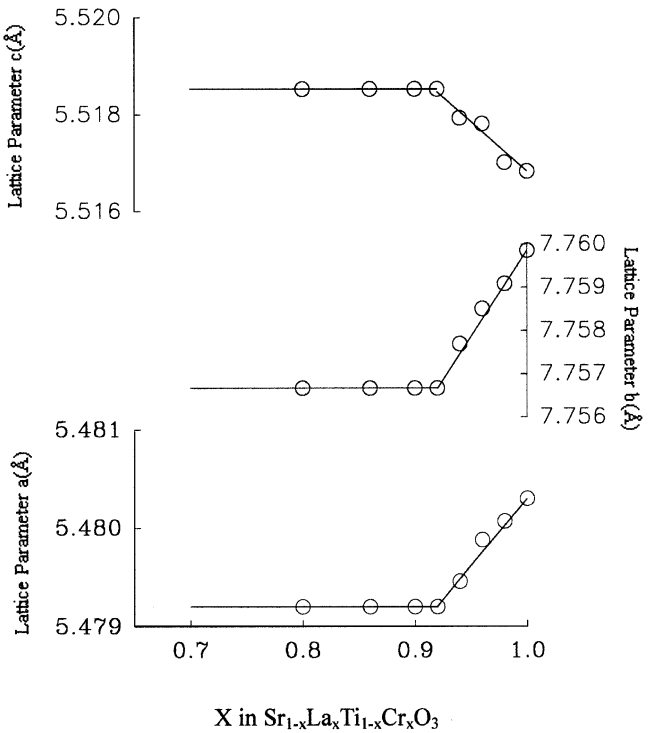

FIG. 10. Variation of the lattice parameters *a*, *b*, and *c* of the orthorhombic phase with the average composition ratio *x*. *x* is the ratio of La/(La + Sr) in the sample.

The bulk conductivity of samples SLTC05–SLTC08 was shown in Fig. 13. They were of rhombohedral structure at room temperature. Their conductivity increased with the increase of La and Cr in the samples. The bulk conductivity activation energies were 0.27, 0.29, 0.26 and 0.25 eV, respectively. One or two of these samples may have had a phase transition during the conductivity testing from 25 to 450°C. However, there was no clear evidence that appeared in the conductivity curves. If all of them were supposed to be rhombohedral during the testing, then the bulk conductivity activation energy for the rhombohedral phase was about 0.27(2) eV. This value was quite similar to 0.28(1) eV for the cubic phase. This meant that if a phase transition between cubic and rhombohedral phase occurred at a certain temperature between 25 and 450°C, the conductivity measurement showed no difference. This might explain the conductive behavior of the sample SLTC04, which had two phases at room temperature.

TABLE 4
The Structure Data of the Orthorhombic Solid Solution $Sr_{1-x}La_xTi_{1-x}Cr_xO_3$

Name	*x*	*a* (Å)	*b* (Å)	*c* (Å)
SLTC16	1.00	5.4803(1)	7.7599(1)	5.5168(1)
SLTC15	0.98	5.4801(1)	7.7591(1)	5.5170(1)
SLTC14	0.96	5.4799(1)	7.7585(1)	5.5178(1)
SLTC13	0.94	5.4795(1)	7.7577(1)	5.5179(1)
SLTC12	0.92	5.4792(1)	7.7567(1)	5.5185(1)

Figure 14 shows the bulk conductivity of samples SLTC09–SLTC11. These samples were of two phases at room temperature. The average bulk conductivity activation energies were 0.25, 0.25 and 0.26 eV, respectively.

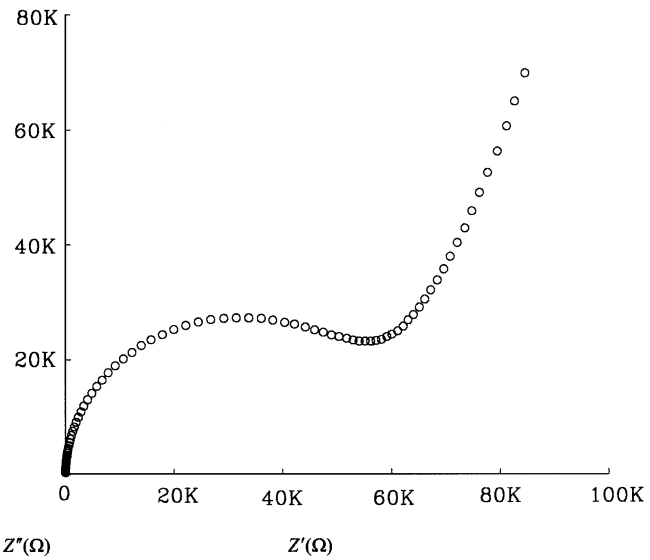

FIG. 11. Typical impedance spectra of $SrTiO_3$ at 350°C.

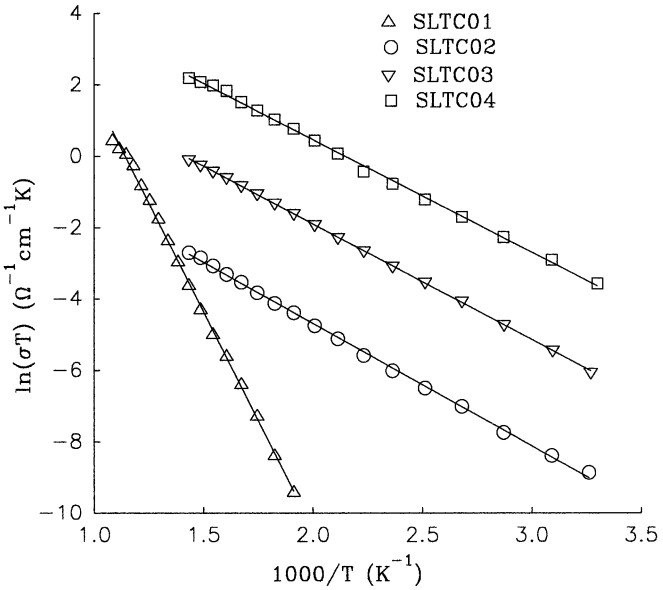

FIG. 12. The conductivity of samples SLTC01–SLTC04 at different temperatures.

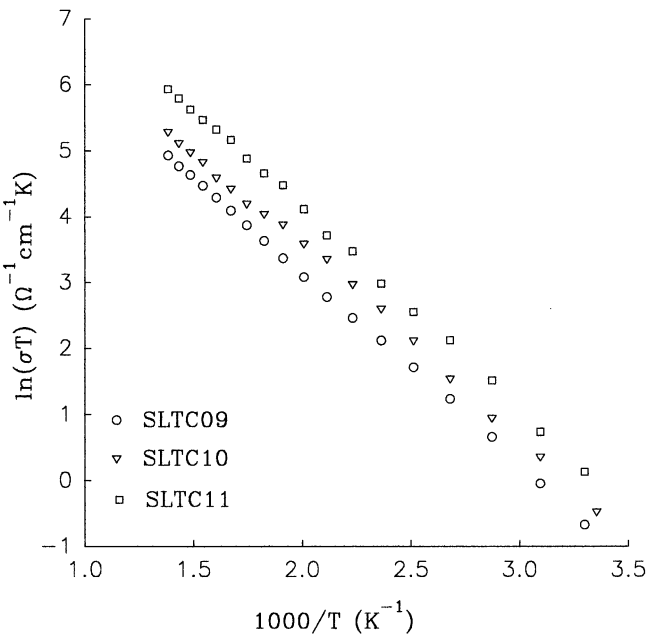

FIG. 14. The conductivity of samples SLTC09–SLTC11 at different temperatures.

Figure 15 shows the bulk conductivity of samples SLTC12–SLTC16. They were of orthorhombic structure at room temperature. For clear presentation, two figures were used. As reported, there was a phase transition between orthorhombic phase and rhombohedral around 260°C (26) for $LaCrO_3$. This phase transition enabled a change on the conductive behavior of the sample SLTC16 ($LaCrO_3$) as shown in Fig. 15A. The bulk conductivity activation energies of the rhombohedral and the orthorhombic phase were 0.19 and 0.24 eV, respectively.

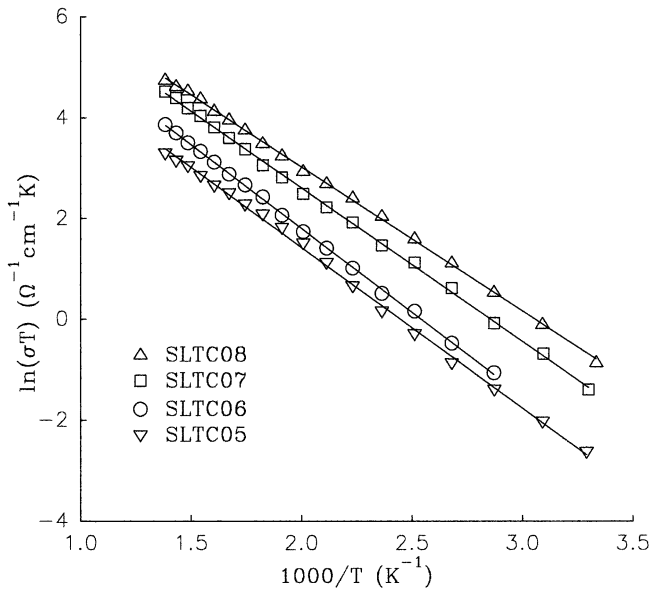

FIG. 13. The conductivity of samples SLTC05–SLTC08 at different temperatures.

It was found that there was also such a change in the conductive behavior for samples SLTC13–SLTC15. It was reasonable to suppose that this change was introduced by the phase transition between the rhombohedral and the orthorhombic phase. With more and more Sr and Ti doped into the $LaCrO_3$, the temperature corresponding to the change of the conductive behavior decreased. The bulk conductivity activation energies were 0.21 eV (rhombohedral) and 0.26 eV (orthorhombic), 0.23 eV (rhombohedral) and 0.32 eV (orthorhombic), 0.21 eV (rhombohedral) and 0.30 eV (orthorhombic) for samples SLTC13–SLTC15, respectively. There was no change observed for the sample SLTC12. The activation energy was 0.21 eV. The conductivity decreased initially when doping Sr and Ti into $LaCrO_3$, then increased with the increase of dopants.

5. CONCLUSIONS

The series $Sr_{1-x}La_xTi_{1-x}Cr_xO_3$ $(0 \le x \le 1)$ has been synthesized at 1500°C for about 60 h. At room temperature, there were three solid solutions: cubic solid solution $Sr_{1-x}La_xTi_{1-x}Cr_xO_3$ $(0 \le x \le 0.168)$, rhombohedral solid solution $Sr_{1-x}La_xTi_{1-x}Cr_xO_3$ $(0.23 \le x \le 0.67)$, and orthorhombic solid solution $Sr_{1-x}La_xTi_{1-x}Cr_xO_3$ $(0.92 \le x \le 1)$. The relationship between the lattice parameters and the composition of the solid solutions agreed well with Vegard's law. The volume per ABO_3 decreased

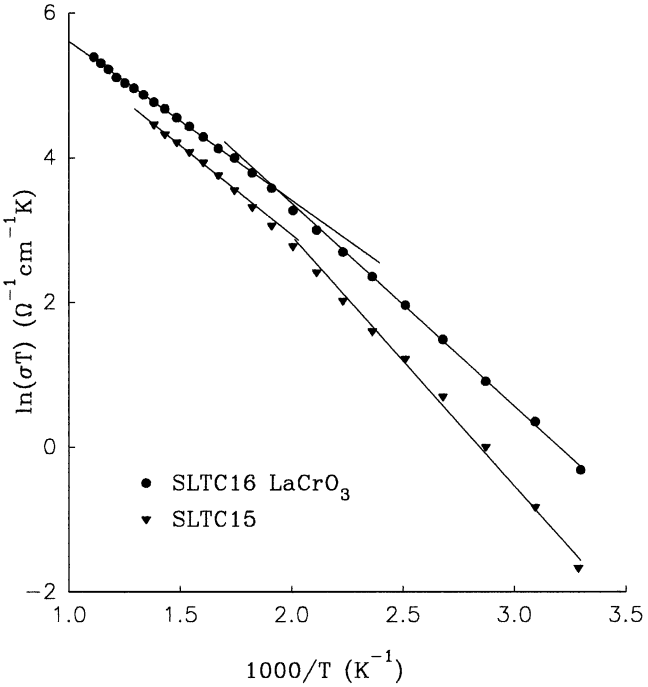

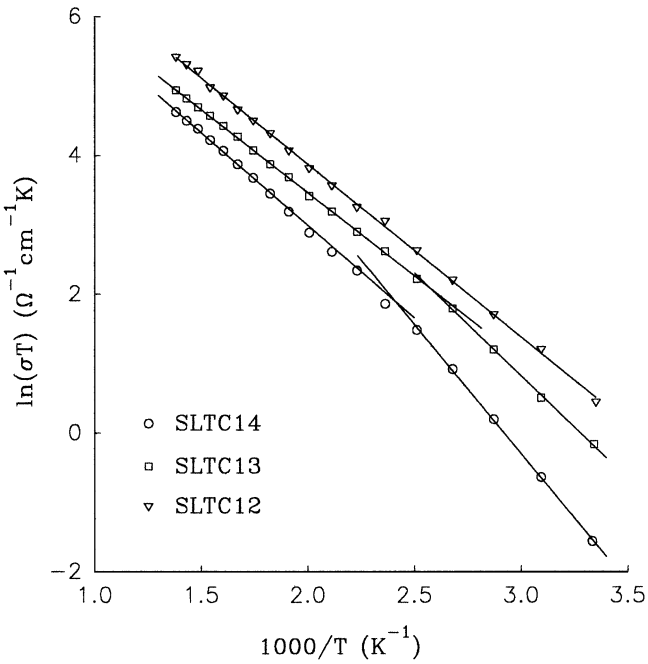

FIG. 15. The conductivity of samples SLTC12–SLTC16 at different temperatures.

with the increase of the ratio La/(La + Sr) in the samples for the cubic and rhombohedral solid solutions, and slowly increased for the orthorhombic solid solution, as shown in Fig. 16.

The conductivity of this series was measured. After doping with $LaCrO_3$, the conductivity of the samples increased around room temperature. This meant that this series was not fit for use as dielectric materials.

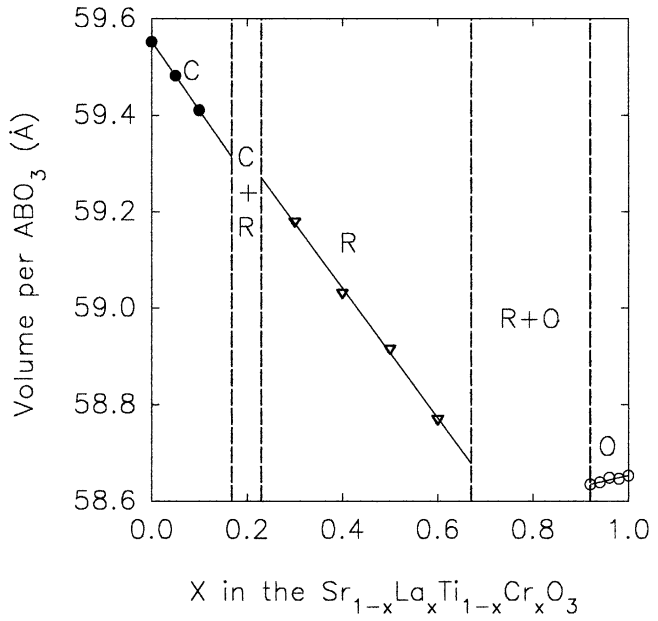

FIG. 16. The comparison of the volume per ABO_3 of three solid solutions in the series $Sr_{1-x}La_xTi_{1-x}Cr_xO_3$. C, cubic solid solution; R, rhombohedral solid solution; and O, orthorhombic solid solution.

ACKNOWLEDGMENTS

We thank the International Exchange Office of Waseda University and Peking University for establishing the cooperation research. The support by the grant-in-aid for Research and Development of New Technology of the Association of Private Universities in Japan is gratefully acknowledged.

REFERENCES

1. C. Frenzel and E. Hegebarth, *Phys. Status Solidi A* **23,** 517 (1974).
2. T. Mitsui and W. B. Westphal, *Phys. Rev.* **124,** 1354 (1961).
3. J. G. Bednos and K. A. Muller, *Phys. Rev. Lett.* **52,** 2289 (1984).
4. G. I. Skanavi, I. M. Ksendzov, V. A. Trigubenko, and V. G. Prokhvatilov, *Sov. Phys. JETP* **6,** 250 (1958).
5. Chen Ang, Zhi Yu, P. M. Vilarinho, and J. L. Baptista, *Phys. Rev. B* **57,** 7403 (1998).
6. G. A. Smolenskii, V. A. Isupov, V. I. Agranovskaya, and S. V. Popov, *Sov. Phys. Solid State* **2,** 2584 (1967).
7. A. N. Gubkin, A. M. Kashtanova, and G. I. Skanavi, *Sov. Phys. Solid State* **3,** 807 (1961).
8. Chen Ang, Zhi Yu, J. Hemberger, P. Lukenheimer, and A. Loidl, *Phys. Rev. B* **59,** 6665 (1999).
9. Chen Ang, Zhi Yu, J. Hemberger, P. Lukenheimer, and A. Loidl, *Phys. Rev. B.* **59,** 6670 (1999).
10. R. K. Dwivedi, D. Kumar, and O. Parkash, *J. Phys. D: Appl. Phys.* **33,** 88 (2000).
11. O. Parkash, L. Pandey, M. K. Sharma, and D. Kumar, *J. Mater. Sci.* **24,** 4505 (1989).

12. R. H. Mitchell and A. R. Chakhmouradian, *J. Solid State Chem.* **144,** 81 (1999).
13. B. J. Kennedy, C. J. Howard, G. J. Thorogood, M. A. T. Mestre, and J. R. Hester, *J. Solid State Chem.* **155,** 455–457 (2000).
14. H. Unoki and T. Sakudo, *J. Phys. Soc. Jpn* **23,** 546 (1967).
15. H. F. Swanson, *Natl. Bur. Stand.* (*U.S.*) *Circ.* **539,** 44 (1953).
16. L. Vegard, *Z. Phys.* **5,** 17 (1921).
17. L. Vegard, *Z. Kristallogr.* **67,** 239 (1928).
18. S. Geller and V. B. Bala, *Acta Crystallogr.* **9,** 1019 (1956).
19. S. Geller, *Acta Crystallogr.* **10,** 243 (1957).
20. C. P. Khattak and D. E. Cox, *Mater. Res. Bull.* **12,** 463 (1977).
21. M. Stojanovic, R. G. Haverkamp, C. A. Mims, H. Moudallal, and A. J. Jacobson, *J. Catal.* **165,** 324 (1997).
22. K. Tezuka, Y. Hinatsu, A. Nakamula, T. Inami, Y. Shimojo, and Y. Morii, *J. Solid State Chem.* **141,** 404 (1998).
23. J. C. C. Abrantes, J. A. Labrincha, and J. R. Frade, *Mater. Res. Bull.* **35,** 955–964 (2000).
24. B. A. Boukamp, *Solid State Ionics* **11,** 39 (1984).
25. J. C. C. Abrantes, J. A. Labrincha, and J. R. Frade, *Mater. Res. Bull.* **35,** 965–976 (2000).
26. T. Hashimoto, N. Tsuzuki, A. Kishi, K. Takagi, K. Tsuda, M. Tanaka, K. Oikawa, T. Kamiyama, K. Yoshida, H. Tagawa, and M. Dokiya, *Solid State Ionics* **132,** 183–190 (2000).